Available online at www.sciencedirect.com

ScienceDirect

journal homepage: www.elsevier.com/locate/he

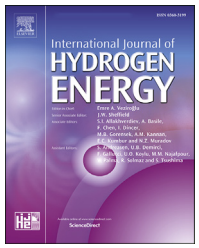

Mechanism of action of polytetrafluoroethylene binder on the performance and durability of high-temperature polymer electrolyte fuel cells

Shuai Liu [a], *Klaus Wippermann* [a], *Werner Lehnert* [a,b,*]

[a] *Institute of Energy and Climate Research, IEK-14: Electrochemical Process Engineering, Forschungszentrum Jülich GmbH, D-52425, Jülich, Germany*

[b] *Modeling in Electrochemical Process Engineering, RWTH Aachen University, D-52056, Aachen, Germany*

HIGHLIGHTS

- The PTFE binder impacts phosphoric acid distribution in the catalyst layer.
- A transmission line equivalent circuit model is applied to fit the EIS data.
- The Pt (100) edge and corner sites are significantly covered by PTFE and phosphate.
- The effect of PTFE bind on the durability of HT-PEFCs is investigated.
- The PTFE network structure helps to reduce phosphoric acid leaching.

ARTICLE INFO

Article history:
Received 19 April 2020
Received in revised form
21 January 2021
Accepted 25 January 2021
Available online 18 February 2021

Keywords:
High temperature polymer electrolyte fuel cell
Polytetrafluoroethylene
Cathode
Accelerated stress test
Phosphoric acid leaching

ABSTRACT

In this work, new insights into impacts of the polytetrafluoroethylene (PTFE) binder on high temperature polymer electrolyte fuel cells (HT-PEFCs) are provided by means of various characterizations and accelerated stress tests. Cathodes with PTFE contents from 0 wt% to 60 wt% were fabricated and compared using electrochemical measurements. The results indicate that the cell with 10 wt% PTFE in the cathode catalyst layer (CCL) shows the best performance due to having the lowest mass transport resistance and cathode protonic resistance. Moreover, cyclic voltammograms show that Pt (100) edge and corner sites are significantly covered by PTFE and phosphate anions when the PTFE content is higher than 25 wt%. Open-circuit and low load-cycling conditions are applied to accelerate degradation processes of the HT-PEFCs. The PTFE binder shows a network structure in the pores of the catalyst layer, which reduces phosphoric acid leaching during the aging tests. In addition, the high binder HT-PEFCs more easily suffer from a mass transport problem, leading to more severe performance degradation.

* *Corresponding author*. Institute of Energy and Climate Research, IEK-14: Electrochemical Process Engineering, Forschungszentrum Jülich GmbH, D-52425, Jülich, Germany.
E-mail address: w.lehnert@fz-juelich.de (W. Lehnert).

https://doi.org/10.1016/j.ijhydene.2021.01.192

Introduction

High-temperature (140–180 °C) polymer electrolyte fuel cells (HT-PEFCs) are considered to exhibit improved tolerance to impurities, easier heat rejection and water management compared to classic PEFCs (usually below 80 °C) [1–4]. However, several issues still exist that impede the commercialization of HT-PEFCs. One of the biggest challenges lies in the cathode, i.e., required high Pt loading, low cathode performance and high catalyst corrosion [5–7]. To reduce the cost and improve the activity of catalysts to the ORR in HT-PEFCs, non-noble metal and platinum alloys catalysts have been investigated by several authors [8–10]. Some of the novel catalysts exhibit higher activity towards ORR, but obviously lower electrochemical stability compared to the commercial Pt/C catalyst.

Optimizations of cathode morphology by employing different binders are effective ways to reduce Pt loading and improve HT-PEFCs' performance. In early HT-PEFC models, polybenzimidazole (PBI), as an amorphous basic polymer, is the most commonly used binder in the catalyst layer due to the high thermal stability and easy reaction with PA [11]. However, additional PBI polymers in the catalyst layer could cause increased mass transport resistance due to the film formed on the Pt/C catalyst and the PA flooding effect [12]. Su et al. compared the performance of gas diffusion electrodes (GDEs) with different kinds of binders, including PBI, polytetrafluoroethylene (PTFE), polyvinylidene difluoride (PVDF) and Nafion [13]. The results demonstrate that GDEs with PTFE and PVDF have better electrochemical performance and stability. The high hydrophobicity is one of the most important properties of PTFE [14], which obviously affects HT-PEFCs' performance in three respects: 1) the PA flooding effect is alleviated, thus leading to an enhancement of gas transport [15,16]; 2) there is no interaction with the phosphoric acid (PA), resulting in high kinetic overpotential [17]; and 3) there is a significant impact on PA leaching [18]. Another influential property of PTFE is the non-conductivity, which 1) decreases the electronic conductivity of GDEs; 2) blocks the active sites and therefore decreases the active area of the catalyst particles [19]; and 3) affects the mechanical stability of GDEs [20]. Moreover, the content of PTFE has a strong impact on the performance of GDEs. Jeong et al. reported that the GDE with a content of 20 wt% PTFE has optimal pore structures and exhibits the best electrochemical performance [21]. Avcioglu et al. noted that even low amounts of PTFE in GDEs could reduce the Pt utilization and lead to reduced performance [22]. Martin et al. state that the absence of PTFE is beneficial for HT-PEFC performance, particularly under high load operations [23]. These works provide different PTFE contents for electrode optimization. It is still of great significance to further study the mechanism of action of PTFE on the electrochemical performance of HT-PEFCs. Moreover, the durability of cathodes with different contents of PTFE binder has not been widely investigated.

Accelerated stress tests (ASTs) are an effective method to provoke degradation in membrane electrolyte assemblies (MEAs) on a short time scale so as to study the effect of a component on the degradation of HT-PEFCs [24–26]. The high potential, especially the open-circuit condition, has proven to be one of the most destructive factors in affecting HT-PEFC durability. Park et al. conducted an accelerated stress test at a high potential of 1.2 V to analyze the degradation of a Pt catalyst and novel carbon-based support [27]. Meanwhile, Zhao et al. applied open circuit voltage conditions as a stressor to investigate and compare the degradation of three different composite membranes [28]. Moreover, the low load operating mode is frequently used as an effective stressor for accelerated testing [29,30]. Søndergaard et al. applied an AST protocol of potential cycling to investigate the effect of humidification on catalyst durability [31]. Similarly, Schonvogel et al. carried out an experiment on HT-PEFCs under load cycling to accelerated PA leaching and catalyst degradation [32]. Accordingly, OCV and low load cycling conditions can be applied to accelerate the degradation process and compare the aging behavior of HT-PEFCs with different PTFE contents.

For this work, gas diffusion electrodes with different PTFE contents from 0 wt% to 60 wt% were fabricated and characterized by the techniques that include scanning electron microscopy (SEM), energy dispersive X-ray (EDX), Brunauer-Emmett-Teller (BET) analysis, polarization curves, electrochemical impedance spectroscopy (EIS) and cyclic voltammetry (CV). In addition, ASTs (i.e., OCV and low load cycling) are applied to HT-PEFCs with different PTFE contents. The degradation rates of the cells are compared and the loss rates of Pt and PA are measured by means of inductively coupled plasma mass spectrometry (ICP-MS).

Experimental

Preparation of single cell HT-PEFCs

The GDEs were prepared using a doctor blade method. The preparation process of a GDE is as follows: First, 1 g of a carbon-supported Pt catalyst (20 wt% Pt, Alfa Aesar) was mixed with 3.0 mL of deionized water and 19.5 mL of isopropanol solvent, and then the mixture was sonicated for 4 min. Secondly, the necessary amount of PTFE, purchased from Dyneon TF5032Z, was added in the ink, which was then sonicated for 30 min to finely disperse the Pt/C catalyst and binder in the solvent. Thirdly, the ink was coated in a commercially-available gas diffusion layer (GDL), with a microporous layer on one side (Freudenberg H2315C2), by a blade with a speed of 7.5 mm s^{-1}. Finally, the prepared GDEs were dried in a fume hood overnight at 25 °C and cut into the requisite size before use. The PTFE content in the anode was maintained at 40 wt%, with a Pt loading of 0.6 ± 0.05 mg cm^{-2} and a thickness of 60 ± 10 μm. The cathodes of different binder contents were prepared by using different spacers and recipes of the ink, with the platinum loading maintained at 1.1 ± 0.1 mg cm^{-2}. The parameters of the cathode catalyst layers (CCLs) and recipes are shown in Table 1.

A cross-linked AM-55 membrane purchased from FuMA-Tech GmbH/Germany was used in this work. The membrane was immersed in the 85 wt% PA at 110 °C for around 18 h under magnetic stirring to reach a PA doping level of 15 ± 0.5 mg cm^{-2} (approximately 11 mol per PBI unit) [33]. The home-made MEA was made by sandwiching the membrane

Table 1 – Parameters and recipes for the preparation of the CCLs.

PTFE content/wt.%	Electrode Thickness/μm	Pt loading/mg cm^{-2}	Pt/C catalyst/g	Water/mL	Solvent/mL	PTFE solution/μL	Thickness of spacer/cm
0	95	1.15	1.0	1.9	12.7	0	0.7
5	106	1.17	1.0	2.2	14.6	58	0.8
10	103	1.18	1.0	2.4	15.6	74	0.8
25	130	1.16	1.0	2.7	17.5	364	0.9
40	139	1.12	1.0	3.0	19.5	741	1.0
60	163	1.07	1.0	3.6	23.4	1670	1.3

between the anode and cathode and then assembled in a single HT-PEFC cell. During the HT-PEFC assembly process, the torque applied to each bolt was typically 6 Nm to prevent a gas leakage. Finally, the HT-PEFCs went through a gas leakage test: 1) purging nitrogen on both sides until the pressure was around 300 mbar and then closing the inlet and outlet; 2) recording the pressure drop within 1 min. The gas sealing of the HT-PEFCs only meets the requirement when the pressure drop was lower than 40 mbar.

The outermost components of an HT-PEFC were endplates made of stainless steel, with a gas inlet and outlet on them. Next to the endplates were expanded graphite (Sigraflex ®) used for sealing and conducting. The next components were three-channel serpentine flow fields made of graphite with a width of 1 mm for the ribs and channels. The home-made MEA was sandwiched by the flow fields and the outside of the MEA were perfluoroalkoxy gaskets, which are used for gas sealing and as a hard stop to achieve 15–20% MEA compression.

Electrochemical measurements

After the assembly and gas leakage testing procedures, the HT-PEFCs were investigated on an automated test station. At first, a break-in procedure was carried out by running at 200 mA cm^{-2} for 70 h, with the anode and cathode supplied with non-humidified pure H_2 and air, respectively, at a stoichiometry of 2/2. Then, the polarization curve was recorded galvanostatically by increasing the current density in steps of either 10 or 50 mA cm^{-2} every 2 min, depending on whether the current density was below or above 100 mA cm^{-2}, up to the maximum current density of 800 mA cm^{-2}.

The cathode EIS and CV measurements were conducted by an IM 6 unit from Zahner-Elektrik. During the in-situ measurements, the anode served as both the counter electrode and the quasi-reference electrode; the cathode functioned as the working electrode [32,34–36]. Before EIS measurements, HT-PEFCs were kept at the desired current densities (i.e., 200 mA cm^{-2}) at 160 °C for 15 min to reach a steady state, and then the Nyquist plots were recorded and fitted using the THALES software. After that, the current load was switched off for the CV tests. The anode and cathode were then supplied with hydrogen and nitrogen with flow rates of 4.6 mL min^{-1} cm^{-2} and 6.9 mL min^{-1} cm^{-2}, respectively. Five cycles of CVs were measured between 0.05 V and 1.2 V at a scan rate of 50 mV s^{-1}, with the last cycle chosen for the evaluation of the electrochemical catalyst surface area (ECSA). The ECSA value was estimated according to the hydrogen desorption charge on the electrode [35–38].

Ex-situ characterization methods

SEM and EDX mapping images of the prepared GDEs were taken on a Zeiss Gemini Ultra Plus microscope. To compare the PA leaching and Pt loss inside the GDEs with the amount discharged from the MEA, the exhaust water was collected from the cathode side by cooling the gas stream down to 7 °C. The concentrations of PO_4^{3-} and Pt in the water were measured by ICP-MS. Phosphate was then determined by a continuous flow analysis. The relative errors were 8%, 5% and 2% for concentrations <0.5 μg mL^{-1}, 0.5–1 μg mL^{-1} and 1–3 μg mL^{-1}, respectively. For Pt detection, three replicate dilutions of each sample were prepared and analyzed. Due to the small Pt concentration in the collected water near the limit of detection, the standard deviation is relatively large. The specific surface areas of the CCLs with different PTFE contents were measured by a Micromeritics Gemini VII device with a software V1.03t. The Barrett-Joiner-Halenda desorption analysis was used to determine the pore sizes below 30 nm, with the BET values having an error of up to 10%.

Results and discussion

BET and SEM of the catalyst layer

To investigate the effect of the PTFE content on the pore size distribution of the catalyst layer, a fresh catalyst was scraped off the GDL and tested using the BET method. Fig. 1A shows the differential pore volume of pores smaller than 50 nm. Above 4.0 nm, the samples show a similar pore size distribution, only shifted due to the different BET areas. Comparing all samples, only minor differences are found up to a pore diameter of 10 nm diameter. The most striking differences were in the pore diameter range between 1.5 nm and 3.0 nm, with the maximum deviation occurring around 2.2 nm. The BET values of the CCLs are presented in Fig. 1B. It can be seen that the surface area and pore volume decrease with increasing PTFE content in the CCLs.

It has been reported that the pores with the size <100 nm are termed as the primary pores and >100 nm termed as the secondary pores [39]. The primary pores account for 5%–10% of the total pore volume and a decreased volume of primary pores can lead to an increase in the cathode protonic resistance [40,41]. In Fig. 1B, the reduced BET value of the MEA with more PTFE contents is mainly caused by the blockage of the secondary pores, which may result in a gas transport problem;

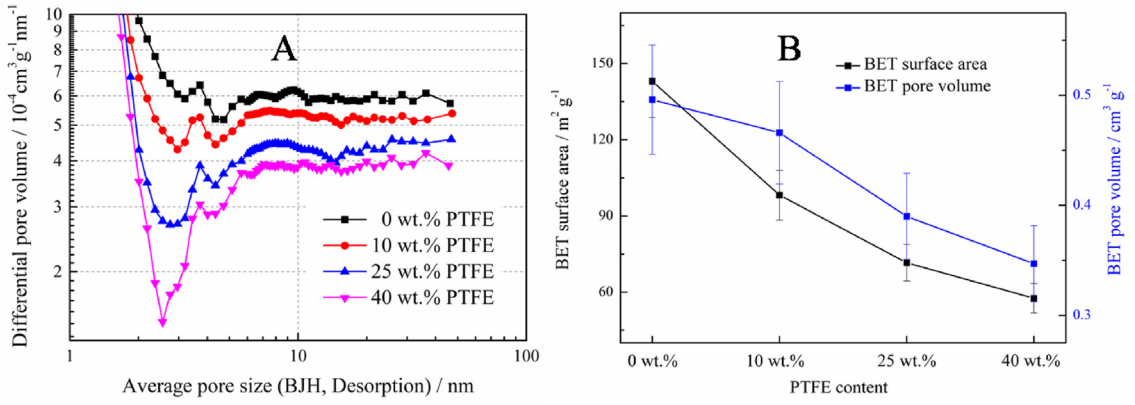

Fig. 1 – (A) Average pore size distribution of the CCLs with different PTFE contents; (B) BET values of the CCLs.

and affect the process of the oxygen reduction reaction (ORR), as the ORR mainly occurs in the secondary pores [42].

The 10 wt% and 40 wt% PTFE GDEs are characterized by SEM and EDX mapping to investigate the effect of PTFE on the morphology of the catalyst layer. It can be seen in the SEM cross-sectional images (Fig. 2A and B) that compared to the high binder (40 wt% PTFE) catalyst layer, the low binder (10 wt % PTFE) CCL shows more homogeneous distributions of PTFE and Pt. Fig. 2C and D exhibit the SEM topography images of the GDEs. PTFE agglomerations are observed in the high binder GDE, and the PTFE binder exhibits a cross-linked network structure in the pores. Furthermore, by comparing the higher magnification (scale bar, 200 nm) images, as shown in Fig. 2E and F, it would seem that the high binder catalyst layer exhibits a more compact structure, which is consistent with the lower BET value.

Comparison of electrochemical properties

Polarization curves

Figure. 3 shows the polarization curves of the HT-PEFCs of different PTFE contents in the CCLs. It can be seen that there are moderate differences in the cells' performance in the so-called Tafel region (j < 0.1 A cm^{-2}), implying that PTFE can affect the kinetics of the ORR on the cathode side. The differences in the curves increase at higher current densities. The HT-PEFC with 60 wt% PTFE in the CCL exhibits considerably lower performance than the other HT-PEFCs, while the 10 wt% PTFE HT-PEFC exhibits the best electrochemical performance.

Generally, the cell voltage can be described as follows [43]:

$$E_{iR-free} = E_{cell} + \eta_{ohm} = E_{rev\,(P_{H_2},\ P_{O_2},T)} - \eta_{act} - \eta_{conc} \quad (1)$$

where $E_{iR\text{-}free}$ is the cell voltage compensated for the iR drop, E_{cell} the recorded cell voltage, E_{rev} the reversible potential, η_{act} the activation overpotential, η_{ohm} the ohmic overpotential and η_{conc} the concentration overpotential.

In the Tafel region of the UI curves (j < 0.1 A cm^{-2}), the η_{conc} can be neglected and the potential dependent current density can simply be expressed by the Butler-Volmer equation [44,45]:

$$j = j_0\left[e^{\frac{\alpha n F \eta_{act}}{RT}} - e^{-\frac{(1-\alpha) n F \eta_{act}}{RT}}\right] \quad (2)$$

where j_0 is the exchange current density, n the number of electrons, η_{act} the activation overpotential, and α the charge transfer coefficient.

An increase in the current results in an increased η_{act}, which leads to either the forward reaction or reverse reaction to dominate the process [46]. This is supported by the fairly linear Tafel slopes obtained in the current density range of 10–100 mA/cm^2 (see Fig. 3B). Therefore, Equation (2) is simplified as:

$$j = j_0 e^{\frac{\alpha n F \eta_{act}}{RT}} \quad (3)$$

The simplified equation is transferred to the Tafel equation:

$$\eta_{act} = a + b\lg j \quad (4)$$

where a is a constant and b is the so-called Tafel slope.

Beneath the exchange current density, the Tafel slope is another important indicator for the rate of electrode reaction kinetics. At constant operation conditions, lower Tafel slopes mean faster electrode reactions, like oxygen reduction on the cathode catalyst [47]. Fig. 3B shows the η_{act}-$lg(j)$ graph in the Tafel region from 0.01 A cm^{-2} to 0.1 A cm^{-2}. Table 2 shows the calculated Tafel slopes and voltages at 200 mA cm^{-2} of the cells. It can be seen that the cells with 40 wt% and 60 wt% PTFE exhibits higher Tafel slope values than the other cells, demonstrating that the ORR kinetics are negatively affected by an excessive amount of PTFE. In this case, the PA distribution in the CCLs is different due to the different hydrophobicity levels of the catalyst layers, probably leading to changes in the ORR path or even causing changes in the Tafel slope [47]. Moreover, PTFE partially covers the Pt/C catalyst and thus leads to a decreased ECSA value, resulting in both an increased charge transfer resistance and Tafel slope [48]. The result of Tafel slopes is consistent with that of the cathode protonic resistance (R_p) (i.e., the 40 wt% and 60 wt% PTFE cells exhibit obvious higher R_p values than the other cells), which will be detailedly discussed later. In Table 2, the cell without

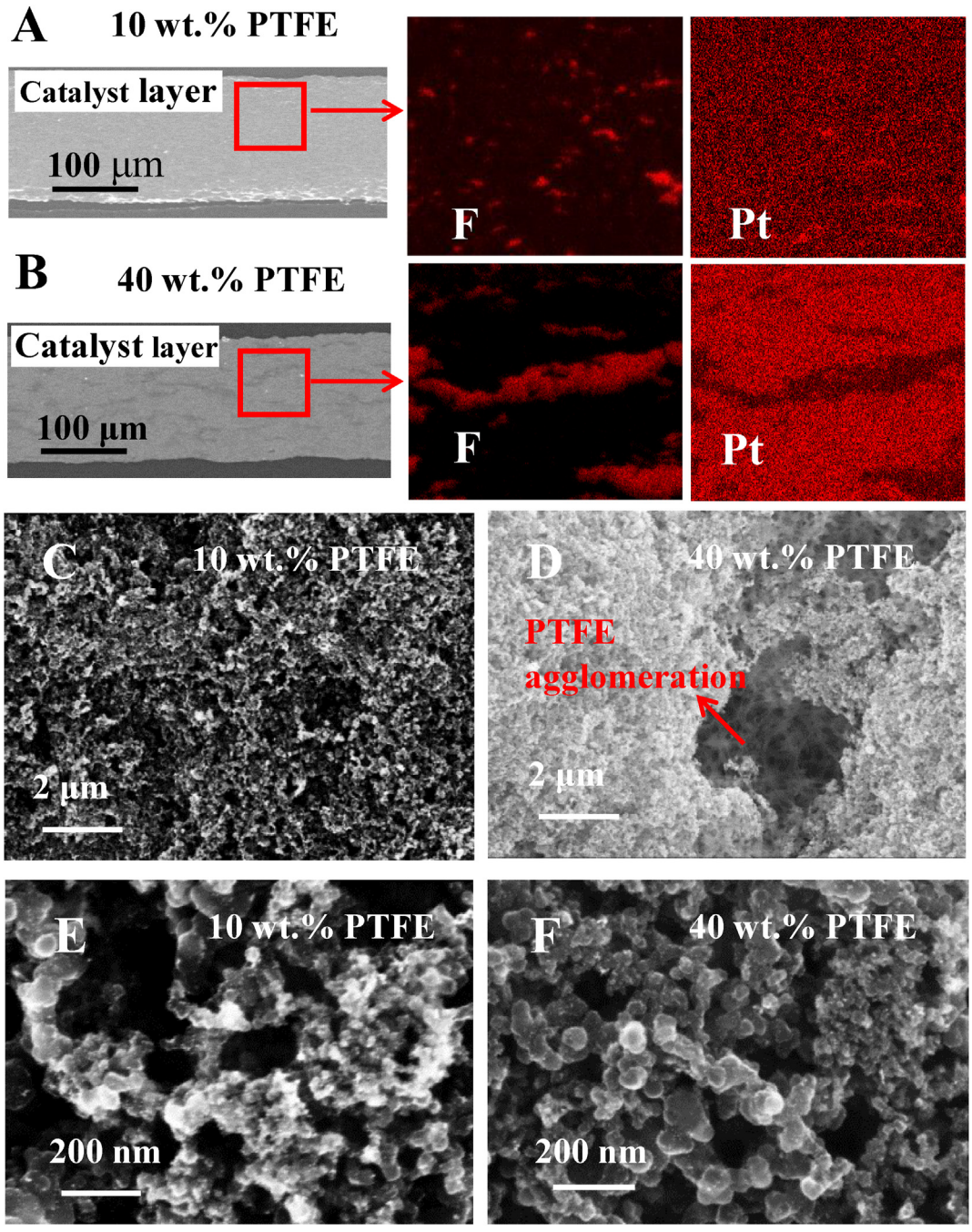

Fig. 2 – (A and B) Cross-sectional SEM and EDX mapping images and (C and D) SEM topography images of the 10 wt% and 40 wt% PTFE catalyst layers; (E and F) higher magnification images of the GDEs.

PTFE shows the lowest Tafel slope, but not the best electrochemical performance. This is because that the kinetic part (i.e. the current density region of 10–100 mA cm^{-2}) of the overall performance is not only determined by the Tafel slope, but also by the exchange current density. Due to the hydrophilic surface of the 0 wt% PTFE electrode, PA molecules significantly migrate from the membrane to the CCL, resulting in PA flooding of CCL pores. This means that the flooded parts of the CCL would be more or less 'dead' because of the low oxygen concentration, therefore leading to a decrease in the exchange current density. On the other hand, the PA migration could result in a low PA content in the membrane and thus an increased hydrogen crossover due to a membrane thinning effect [49]. These effects lead to the reduced electrochemical performance of the 0 wt% PTFE cell. Besides, the voltage of the 10 wt% PTFE cell is more than 50 mV higher than that of the 60 wt% PTFE cell at 200 mA cm^{-2} (0.639 V vs. 0.585 V). These results indicate that the binder content of PTFE in the CCL has a considerable influence on HT-PEFCs' performance.

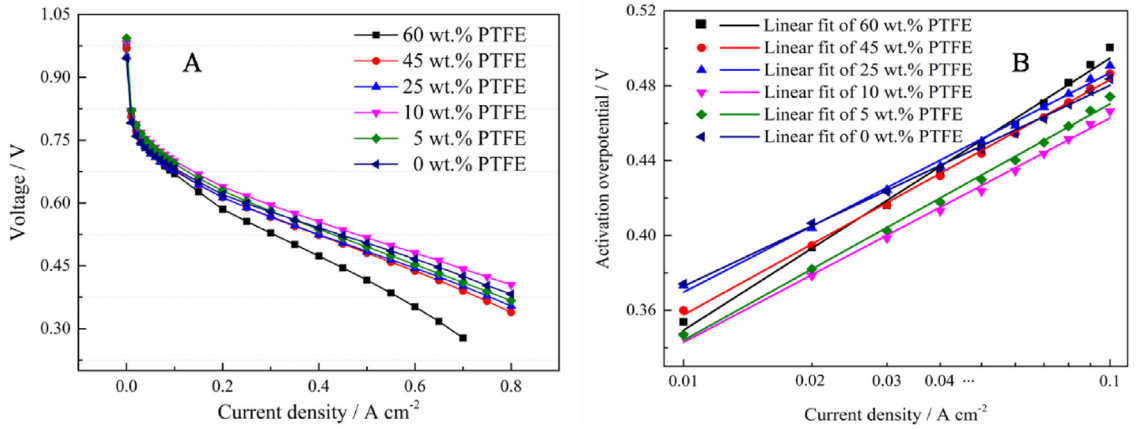

Fig. 3 – (A) Polarization curves of the HT-PEFCs operated at T = 160 °C, stoichiometry: Air/H_2 = 2/2 with different PTFE contents after the 72 h break-in procedure; (B) Tafel plots of the cells in the range from 0.01 A cm^{-2} to 0.1 A cm^{-2}.

Table 2 – Tafel slopes and voltages of the HT-PEFCs at 200 mA cm^{-2}.

PTFE/wt.%	Tafel slope/mV dec^{-1}	Voltage at 200 mA cm^{-2}/V
0	0.095	0.620
5	0.110	0.629
10	0.107	0.639
25	0.112	0.613
40	0.123	0.613
60	0.131	0.585

The optimal PTFE content (10 wt%) is inconsistent with the works of Mack et al. and Jeong et al., which show that the optimal PTFE contents are 5 wt%. and 20 wt%, respectively [19,21]. Table 3 shows the main MEA parameters of these works and our own, indicating that the difference in optimal PTFE contents is probably caused by the different PA doping levels (i.e., a higher doping level needs more PTFE content in the porous catalyst layer to achieve the greatest performance). In addition, the manufacturing technique could also play an important role in the electrode morphology, thus affecting the optimal PTFE content.

CV and EIS measurements

Figure 4A and B shows the cathode CVs of the HT-PEFCs scanned from 50 mV to 1.2 V at a scan rate of 50 mV s^{-1}. The peaks in the red box from 0.1 V to 0.4 V in Fig. 4A are related to hydrogen desorption, which are used to calculate the ECSA of the HT-PEFCs [50]. As is shown in Fig. 4B, it is obvious that the ECSA decreases as the PTFE content increases, with the values of the 0 wt%, 25 wt% and 60 wt% PTFE cells of 18.4 m^2 g^{-1}, 13.8 m^2 g^{-1} and 11.6 m^2 g^{-1}, respectively. This result indicates that the existence of PTFE in the CCL can lead to the blockage of Pt surface. In addition, the peaks at 0.13 V and 0.28 V are assigned to the hydrogen desorption on the Pt (110) site and Pt (100) edge and corner sites, respectively [51]. These two peaks are merged to some extent, due to the adsorption of phosphate anions and the dry operating conditions of HT-PEFCs [52,53].

Figure. 4C and D shows the cathode CVs recorded from 50 mV to 505 mV. The first thing should be noted is that compared to Fig. 4A, the area of the hydrogen desorption peak in Fig. 4C obviously decreases, with the peak current density reducing from approximately 0.025 A cm^{-2} to 0.02 A cm^{-2}. This can be explained by that the upper potential in CVs is too small (505 mV), leading to a deactivation of the electrode because of the cathode poisoning. It means, that the hydrogen desorption charge increases with increasing upper potential until it reaches a saturation value (the true value) at upper potentials higher than 1 V vs. reversible hydrogen electrode.

In Fig. 4D, separate peaks at 0.13 V and 0.28 V are observed, which is different from Fig. 4B that only one peak clearly appears. This is presumably due to the unsaturated hydrogen coverage of the Pt surface, leading to the reduction of the peak of the Pt (110) site, further the separation of the peaks. Moreover, the peak at 0.28 V is small in the cells with 60 wt%, 40 wt% and 25 wt% PTFE in the CCLs. This observation is highly related to two factors. One is the blockage of the Pt (100) site when the PTFE content exceeds 25 wt%. Similar statements have been reported in classic PEFCs [54,55]. Friedmann et al. found that the PTFE binder in CCLs could cause a blockage of active catalyst sites and a decrease in the hydration of the catalyst surface area, thus resulting in lower catalyst utilization and poor proton conductivity [55]. The second is that the increased blocking of the surface (when

Table 3 – Main MEA parameters of the works of Mack et al., Jeong et al. and our own.

First author	PA doping level/mol per PBI unit	Optimal PTFE content	Pt loading/mg cm^{-2}	Manufacturing technique
Mack [19]	5	5%	1.0	Airbrushing
Jeong [21]	29	20%	1.1	Spraying
This work	11	10%	1.1	Doctor blade

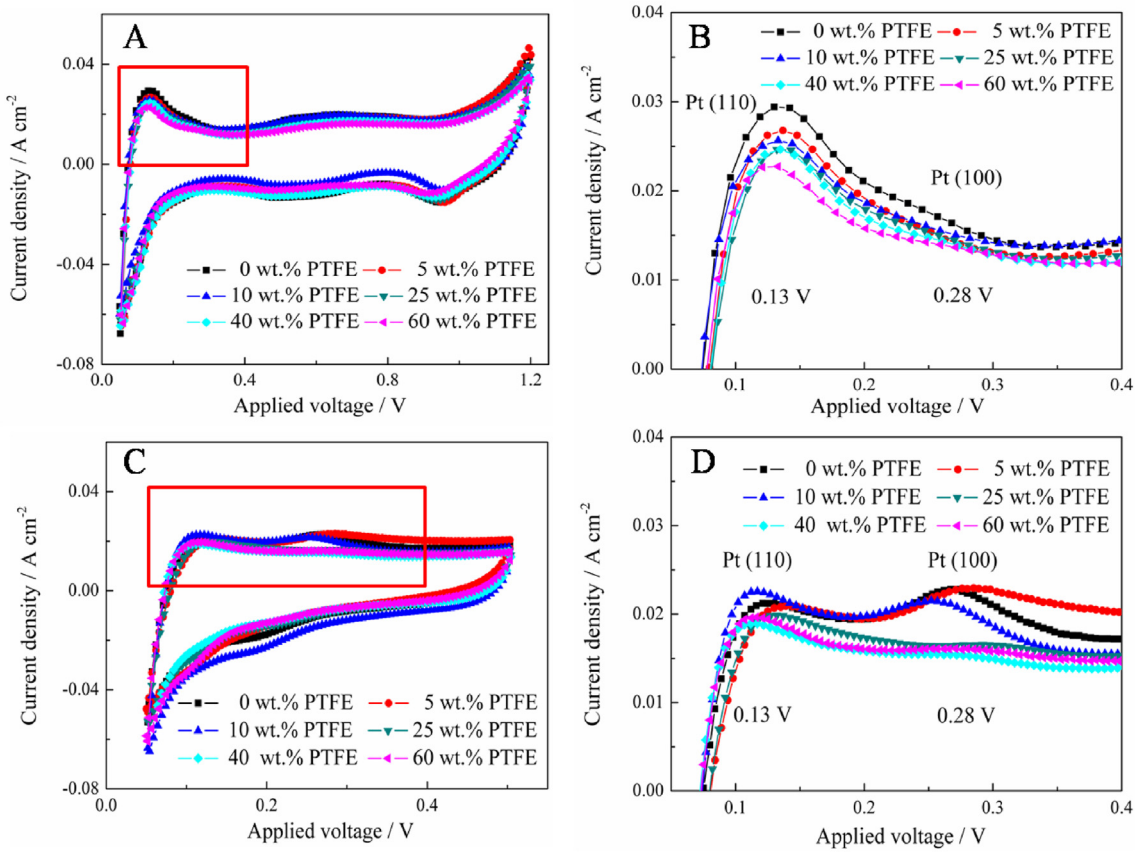

Fig. 4 – (A) Cathode CV curves recorded from 50 mV to 1.2 V at a scan rate of 50 mV s^{-1}, T = 160 °C; (B) magnified area of (A) in the red box; (C) Cathode CV curves recorded from 50 mV to 505 mV at a scan rate of 50 mV s^{-1}; (D) magnified area of (C) in the red box. (For interpretation of the references to color in this figure legend, the reader is referred to the Web version of this article.)

increasing the PTFE content) would affect the cathode poisoning caused by the strong adsorption of phosphate anions on the Pt surface. The blocking of active sites for oxygen adsorption and reduction decreases the ECSA and thus the cathode performance. PTFE decreases the ECSA further, probably by a geometrical blocking of the Pt surface. Thus, with increasing PTFE content, the‚free' surface decreases and the Pt catalysts get more and more vulnerable to phosphate poisoning. A widely-used method to clean an electrode surface from (poisoning) adsorbates like phosphate is cyclic voltammetry. Depending on the potential limits, the removement of phosphate is more or less effective. Because the cleaning effect does not apply to geometrical blocking (e.g. by PTFE), the blocking effects by either phosphate or PTFE can be distinguished by varying e.g. the upper potential limit of the cyclic voltammograms, as shown in Fig. 4: if the scanning potential is in the range of Pt oxidation and beginning oxygen evolution (see Fig. 4A), the cleaning of the Pt surface is much more effective than compared to CVs with an upper potential limit far below Pt oxidation (see Fig. 4C). In the former case, where phosphate is effectively removed, the influence of PTFE blocking dominates. Thus, the ECSA calculated from hydrogen desorption charge decreases with increasing PTFE content. In the latter case, the poor cleaning effect does not only decrease the ECSA as a whole, but leads to a dominating blocking effect of phosphate and the influence of the PTFE content is negligible.

EIS measurements were carried out to investigate the mechanism of action of PTFE on HT-PEFC performance. As is shown in Fig. 5A, Nyquist plots were recorded at 200 mA cm^{-2} and fitted by a transmission line equivalent circuit model. R_Ω is the overall ohmic resistance. The 45° line in the Nyquist plot at higher frequencies is caused by the cathode protonic resistance (R_p), which is simulated by classical transmission line impedance (Z_t) in the THALES software [40,56,57]. The R_p value is calculated by the equation below [58]:

$$R_p = Zt/3 \quad [5]$$

The double layer charging in the PA electrolyte/electrode interface is modeled by a constant phase element (CPE_{dl}); the resistance in parallel to the CPE_{dl} represents the charge transfer resistance (R_{ct}) and the mass transport resistance (R_m) is calculated by the Nernst impedance [59]. The fitting error was kept below 3%.

Figure 5B shows that the R_{ct} values for the different MEAs are comparable. It has been discussed above that the ECSA decreases as the PTFE content increases, which should affect the number of triple-phase boundaries and thus the R_{ct} [60]. The nearly constant R_{ct} value of the HT-PEFCs, in this case, is possibly ascribed to the excessive Pt loading in the CCL

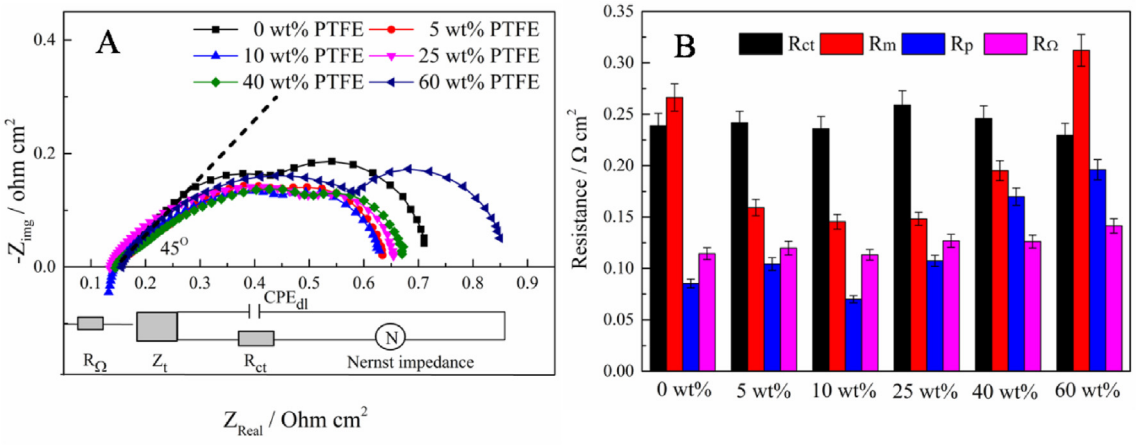

Fig. 5 – (A) Nyquist plots of the HT-PEFCs with different PTFE contents in the CCLs and the equivalent circuit model for EIS data analysis; (B) the corresponding fitting results.

(1.1 ± 0.1 mg cm^{-2}) and the low utilization efficiency of the Pt catalyst [61].

R_m varies significantly with the PTFE content, where the smallest value is obtained at a medium PTFE content of 10 wt %. This indicates at least two opposite effects. PTFE molecules are known to be hydrophobic and thus the increase of R_m at PTFE contents lower than 10 wt% can be explained by an increment of the amount of hydrophilic PA in the CCL. Excessive amounts of PA lead to the PA flooding effect, which hinders the O_2 transport in the porous cathode [62]. At PTFE concentrations higher than 10 wt%, the CCLs are strongly hydrophobic with reduced PA content. Accordingly, PA should have a relatively small effect on the oxygen transport. However, large PTFE agglomerates may block the porous structures in the CCLs, leading to an increase in R_m.

The R_p value remains almost constant when the PTFE content is below 25 wt% and increases dramatically thereafter. This is presumably caused by 1) the decreased volume of primary pores in the CCL with higher PTFE contents (proved by the BET measurements); 2) substantially increased hydrophobicity of the CCLs in the 40 and 60 wt% PTFE cells and thus considerably decreased PA concentrations. Liu et al. state that a large R_p can strongly reduce MEA performance [63]. In our work, the differences in the HT-PEFC performance in the Tafel region are considered to be highly related to the different R_p values.

R_Ω is only little affected by the different PTFE concentrations due to the excess PA doping of the membrane, as a result of which the PA redistribution has no obvious effect on R_Ω. The 60 wt% PTFE cell shows a slightly higher R_Ω than the other cells. This is explained by the fact that the absolute amount of PTFE in the 60 wt% CCL is considerably greater than the other CCLs, with 1670 μL PTFE solution used during the fabricating process (see Table 1). The large amount of non-conductive PTFE causes a decrease in the electron conductivity of the catalyst layer and thus an increased R_Ω [19].

Role of PTFE in HT-PEFC durability

According to the discussion above, the 10 wt% PTFE HT-PEFC shows the optimum electrochemical performance. The effect of PTFE on the durability of HT-PFECs should be another important factor for optimizing the PTFE content.

OCV operation

A 100 h OCV operation is applied to accelerate the degradation of the cells with different PTFE contents in the CCLs (i.e., 10 wt % and 40 wt% PTFE). The voltage-time curves of the aging process are shown in Fig. S1 (see Supplementary Materials), and the 10 wt% and 40 wt% PTFE cells exhibit a similar OCV aging trend, with the degradation rates of 112 μV h^{-1} and 120 μV h^{-1}, respectively. As the OCV loss is considered to be related to the increased hydrogen crossover caused by membrane degradation [64], the similar degradation rate indicates that the PTFE content in the CCL has no effect on the membrane durability. Fig. 6A presents BOL and EOL polarization curves of the HT-PEFCs and it is evident that both cells exhibit pronounced performance degradation. The differences of the BOL and EOL curves are plotted in Fig. 6B. It can be seen that at current densities below 300 mA cm^{-2}, there is only a minor difference in the performance degradation. The difference of the curves increases substantially at higher current densities, with voltage losses of ≈35 mV and ≈61 mV at 800 mA cm^{-2} for the 10 wt% and 40 wt% PTFE cells, respectively. The results signify that the HT-PEFC durability is influenced by the content of PTFE in the CCL.

To further understand the PTFE effect on the performance degradation across the whole current-density range, the UI curves and electrochemical characteristics are analyzed to quantify the voltage loss contributions by Equation (1). Fig. 7 shows the BOL and EOL η_{act} and η_{conc} of the cells. By comparing the η_{act} curves in Fig. 7A, we can see that the η_{act} rises for both cells after aging, and the difference between BOL and EOL increases as the current density increases. The same trend is observed in the η_{conc} of the high binder cell, as shown in Fig. 7B; while the low binder cell exhibits a different changing trend of the η_{conc}, which remains almost constant over the entire current-density range. At 800 mA cm^{-2}, the low binder cell shows a slightly higher increase in η_{act} than the high binder cell (28.7 mV vs. 26.3 mV), while a considerably lower increase in η_{conc} (6.0 mV vs. 34.3 mV). Based on these

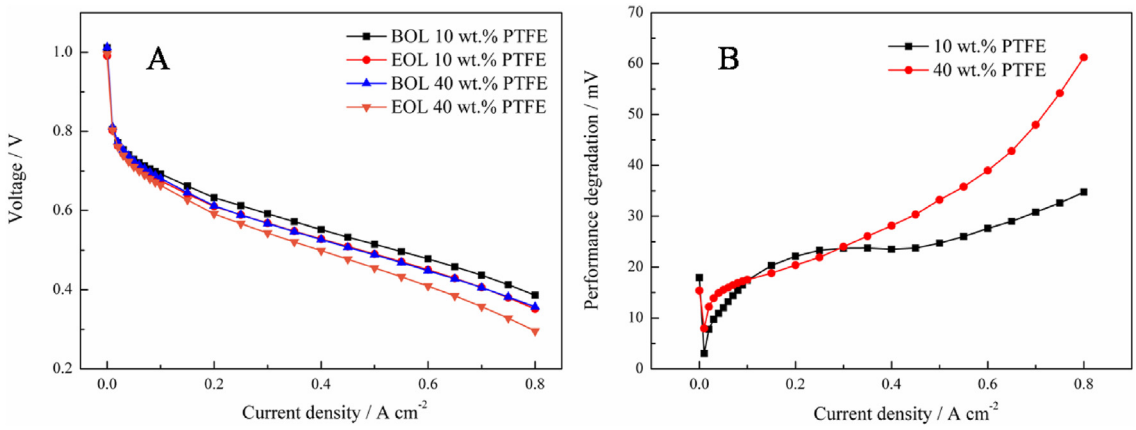

Fig. 6 – (A) BOL and EOL polarization curves of the HT-PTFEs at 160 °C with anode/cathode λ of 2/2; (B) comparison of performance degradation for the HT-PEFCs.

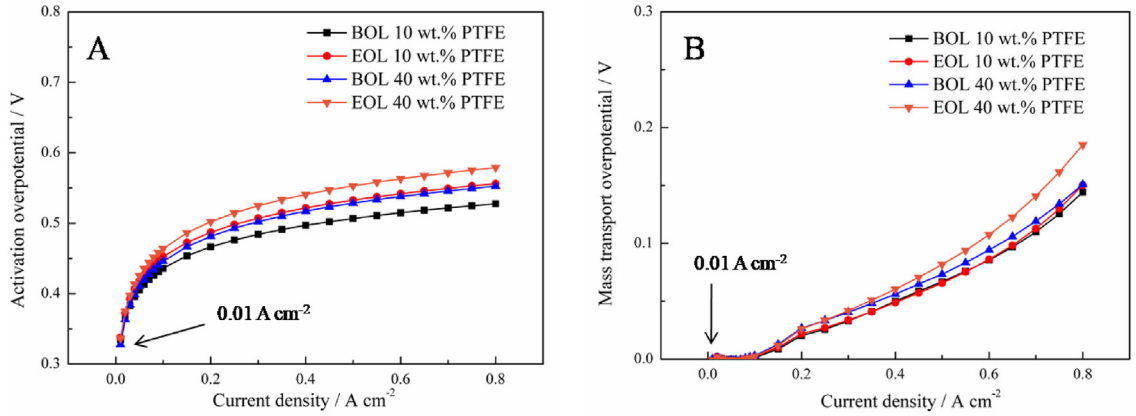

Fig. 7 – (A) Activation overpotential and (B) concentration overpotential of the HT-PEFCs before and after the 100 h OCV operation.

results, it can be concluded that the PTFE binder plays an important role in affecting the gas transport under the stress condition. This can be possibly explained by the fact that severe carbon corrosion/oxidation and PA flooding take place at the cathode during the OCV hold test, which negatively influences the transport of reactant gases [65], and the high binder cell with the less porous and more compact structure is more susceptible to a mass transport problem.

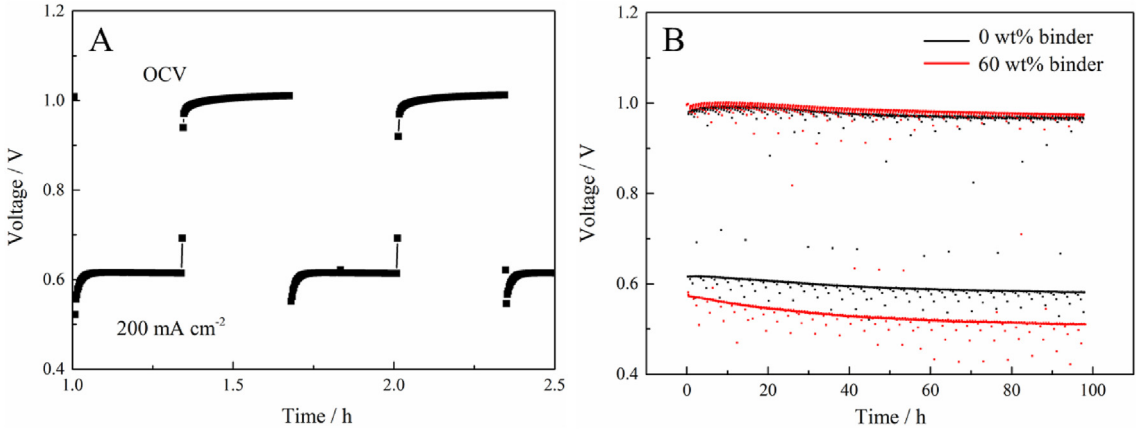

Fig. 8 – (A) Single cycles and (B) voltage-time curves of the 0 wt% and 60 wt% PTFE cells cycling between OCV (20 min) and 200 mA cm^{-2} (20min) for 100 h at 160 °C, H_2/air (λ = 2/2).

Table 4 – Pt and PA concentrations in the water collected from cathode gas stream.

HT-PEFCs	ICP-MS measurement	
	Pt loss	PA loss
0 wt% binder	0.11 μg L^{-1}	1.59 μg mL^{-1}
60 wt% binder	0.07 μg L^{-1}	0.96 μg mL^{-1}

During the OCV operation, HT-PEFCs' performance is influenced by both reversible and irreversible processes [66]. The irreversible degradation is considered to be originated from catalyst agglomeration, carbon corrosion and membrane degradation; reversible degradation is mainly caused by Pt surface oxidation and PA redistribution [28]. It is reported that relatively high load cycling tests can be used to recover cells' performance by removing the effect of reversible processes during the OCV operation [26,66]. To exclude the effect of reversible processes on the voltage drop, the HT-PEFCs are operated under a current cycling profile. As is shown in Fig. S2 (see Supplementary Materials), after the 100 h aging and recovery processes, the performance degradation of the 40 wt% PTFE cell is still considerably higher than that of the 10 wt% PTFE cell when the current density is higher than 300 mA cm^{-2}. These results demonstrate that different PTFE contents of the CCLs can lead to different irreversible degradation behavior in HT-PEFCs.

Low-load cycling test

To further investigate the effect of PTFE content on the PA leaching and Pt loss, the low-load cycling condition was applied as an effective stressor to accelerate the durability test. Due to the limited amount of PA leaching during the 100 h aging at low current densities [67], the experiments were performed by using samples with significant differences in the PTFE content, i.e. 0 and 60 wt%. Fig. 8A shows single cycles of the low load cycling profile, with the current density jumping between OCV and 200 mA cm^{-2} every 20 min. The changes in voltages during the 100 h aging are recorded in Fig. 8B. Compared to the 60 wt% PTFE cell, the 0 wt% PTFE cell shows the same OCV loss rate of 220 μV h^{-1}, while a notably lower voltage loss rate at 200 mA cm^{-2} (340 μV h^{-1} vs. 620 μV h^{-1}). These results are consistent with the 100 h OCV aging test discussed previously, i.e., the lower binder cells show lower performance degradation after the aging tests.

The PA leaching and Pt migration outside the cathodes are compared by ICP-MS. In our previous work, it has been proved that Pt corrosion reaction occurs under the acidic and high-temperature conditions [5], as shown in Equation (6):

$$Pt \rightarrow Pt^{z+} + ze^{-} \quad (6)$$

The Pt loss outside HT-PEFCs with the amount discharged from the MEA is compared. In Table 4, both of the HT-PEFCs exhibit a negligible amount of Pt loss, indicating that catalyst migration outside the cells is not the cause of performance degradation [36]. In addition, the 0 wt% PTFE cell exhibits more severe PA leaching. This is probably due to the observed network structure of the PTFE agglomeration in CCL pores, as is shown in Fig. 2D, which may hold the PA in the CCLs during the cycling tests. Su et al. made a similar statement in Ref. [18]. Due to the short-time operation, the higher PA leaching of the 0 wt% PTFE cell is not reflected on the voltage loss.

Conclusions

In this work, HT-PEFCs with different contents of PTFE binder in the cathode catalyst layers (CCLs) are compared by the ex-situ measurements and electrochemical performance under accelerated test conditions. The results indicate that the charge transfer resistance and the ohmic resistance don't significantly change with different PTFE contents. The PTFE binder influences HT-PEFCs by:

- Adjusting the phosphoric acid (PA) distribution and thus affecting the mass transport resistance and the cathode protonic resistance of the CCLs. The 10 wt% and 25 wt% PTFE cells show the lowest mass transport resistance and cathode protonic resistance. The lack of PTFE in the CCL leads to the PA flooding effect, while excessive PTFE in the CCL causes poor proton conductivity on the CCL.
- Blocking Pt catalyst surface and porous structures, resulting in lower BET values and more compact morphology of the CCL.
- Trapping the impregnated PA in the PTFE network of the CCL, resulting in lower PA leaching in higher binder cells.

According to the experimental results, a relatively low PTFE content (10 wt%) is beneficial for HT-PEFC performance. It should be noted here that the result is based on the short-term running of HT-PEFCs. During long-term operations at high loads, PA leaching becomes a non-negligible issue that influences HT-PEFC durability. In this case, a higher PTFE content of 10 wt%-25 wt% is suggested for the CCL, as PA can be held in the PTFE network structure. This results in a reduced PA loss rate and a more stable Pt catalyst.

Declaration of competing interest

The authors declare that they have no known competing financial interests or personal relationships that could have appeared to influence the work reported in this paper.

Acknowledgments

This work was financially supported by the China Scholarship Council, grant number 201506890023. The authors would like to gratefully thank Mr. Christopher Wood for the careful proofreading of this paper.

Appendix A. Supplementary data

Supplementary data to this article can be found online at https://doi.org/10.1016/j.ijhydene.2021.01.192.

REFERENCES

[1] Di Noto V, Negro E, Sanchez J-Y, Iojoiu C. Structure-relaxation interplay of a new nanostructured membrane based on tetraethylammonium trifluoromethanesulfonate ionic liquid and neutralized nafion 117 for high-temperature fuel cells. J Am Chem Soc 2010;132:2183–95.

[2] Xia L, Zhang C, Hu M, Jiang S, Chin CS, Gao Z, et al. Investigation of parameter effects on the performance of high-temperature PEM fuel cell. Int J Hydrogen Energy 2018;43:23441–9.

[3] Devrim Y, Albostan A, Devrim H. Experimental investigation of CO tolerance in high temperature PEM fuel cells. Int J Hydrogen Energy 2018;43:18672–81.

[4] Xu X, Yang W, Zhuang X, Xu B. Experimental and numerical investigation on effects of cathode flow field configurations in an air-breathing high-temperature PEMFC. Int J Hydrogen Energy 2019;44:25010–20.

[5] Liu S, Rasinski M, Lin Y, Wippermann K, Everwand A, Lehnert W. Effects of constant load operations on platinum bands formation and cathode degradation in high-temperature polymer electrolyte fuel cells. Electrochim Acta 2018;289:354–62.

[6] Bandlamudi V, Bujlo P, Sita C, Pasupathi S. Study on electrode carbon corrosion of high temperature proton exchange membrane fuel cell. Mater Today: Proceedings 2018;5:10602–10.

[7] Devrim Y, Arıca ED. Multi-walled carbon nanotubes decorated by platinum catalyst for high temperature PEM fuel cell. Int J Hydrogen Energy 2019;44:18951–66.

[8] Li Q, Wu G, Cullen DA, More KL, Mack NH, Chung HT, et al. Phosphate-tolerant oxygen reduction catalysts. ACS Catal 2014;4:3193–200.

[9] Parrondo J, Mijangos F, Rambabu B. Platinum/tin oxide/carbon cathode catalyst for high temperature PEM fuel cell. J Power Sources 2010;195:3977–83.

[10] Park H, Kim D-K, Kim H, Oh S, Jung WS, Kim S-K. Binder-coated electrodeposited PtNiCu catalysts for the oxygen reduction reaction in high-temperature polymer electrolyte membrane fuel cells. Appl Surf Sci 2020:510.

[11] Seland F, Berning T, Børresen B, Tunold R. Improving the performance of high-temperature PEM fuel cells based on PBI electrolyte. J Power Sources 2006;160:27–36.

[12] Yusof M, Jalil A, Ahmad A, Triwahyono S, Othman M, Abdullah T, et al. Effect of Pt–Pd/C coupled catalyst loading and polybenzimidazole ionomer binder on oxygen reduction reaction in high-temperature PEMFC. Int J Hydrogen Energy 2019;44:20760–9.

[13] Su H, Pasupathi S, Bladergroen B, Linkov V, Pollet BG. Optimization of gas diffusion electrode for polybenzimidazole-based high temperature proton exchange membrane fuel cell: evaluation of polymer binders in catalyst layer. Int J Hydrogen Energy 2013;38:11370–8.

[14] Lee WJ, Lee JS, Park H-Y, Park HS, Lee SY, Song KH, et al. Improvement of fuel cell performances through the enhanced dispersion of the PTFE binder in electrodes for use in high temperature polymer electrolyte membrane fuel cells. Int J Hydrogen Energy 2020;45:32825–33.

[15] Mazúr P, Soukup J, Paidar M, Bouzek K. Gas diffusion electrodes for high temperature PEM-type fuel cells: role of a polymer binder and method of the catalyst layer deposition. J Appl Electrochem 2011;41:1013–9.

[16] Wannek C, Lehnert W, Mergel J. Membrane electrode assemblies for high-temperature polymer electrolyte fuel cells based on poly (2, 5-benzimidazole) membranes with phosphoric acid impregnation via the catalyst layers. J Power Sources 2009;192:258–66.

[17] Park J, Kwon K, Cho M, Hong S-G, Kim T, Yoo D. Role of binders in high temperature PEMFC electrode. J Electrochem Soc 2011;158:B675–81.

[18] Su H, Pasupathi S, Bladergroen BJ, Linkov V, Pollet BG. Enhanced performance of polybenzimidazole-based high temperature proton exchange membrane fuel cell with gas diffusion electrodes prepared by automatic catalyst spraying under irradiation technique. J Power Sources 2013;242:510–9.

[19] Mack F, Morawietz T, Hiesgen R, Kramer D, Gogel V, Zeis R. Influence of the polytetrafluoroethylene content on the performance of high-temperature polymer electrolyte membrane fuel cell electrodes. Int J Hydrogen Energy 2016;41:7475–83.

[20] Lobato J, Canizares P, Rodrigo M, Ruiz-López C, Linares J. Influence of the Teflon loading in the gas diffusion layer of PBI-based PEM fuel cells. J Appl Electrochem 2008;38:793–802.

[21] Jeong G, Kim M, Han J, Kim H-J, Shul Y-G, Cho E. High-performance membrane-electrode assembly with an optimal polytetrafluoroethylene content for high-temperature polymer electrolyte membrane fuel cells. J Power Sources 2016;323:142–6.

[22] Avcioglu GS, Ficicilar B, Eroglu I. Effect of PTFE nanoparticles in catalyst layer with high Pt loading on PEM fuel cell performance. Int J Hydrogen Energy 2016;41:10010–20.

[23] Martin S, Li Q, Steenberg T, Jensen JO. Binderless electrodes for high-temperature polymer electrolyte membrane fuel cells. J Power Sources 2014;272:559–66.

[24] Stariha S, Macauley N, Sneed BT, Langlois D, More KL, Mukundan R, et al. Recent advances in catalyst accelerated stress tests for polymer electrolyte membrane fuel cells. J Electrochem Soc 2018;165:F492–501.

[25] Taccani R, Chinese T, Boaro M. Effect of accelerated ageing tests on PBI HTPEM fuel cells performance degradation. Int J Hydrogen Energy 2017;42:1875–83.

[26] Thomas S, Jeppesen C, Steenberg T, Araya SS, Vang JR, Kær SK. New load cycling strategy for enhanced durability of high temperature proton exchange membrane fuel cell. Int J Hydrogen Energy 2017;42:27230–40.

[27] Park S, Shao Y, Kou R, Viswanathan VV, Towne SA, Rieke PC, et al. Polarization losses under accelerated stress test using multiwalled carbon nanotube supported Pt catalyst in PEM fuel cells. J Electrochem Soc 2011;158:B297–302.

[28] Zhao M, Shi W, Wu B, Liu W, Liu J, Xing D, et al. Influence of membrane thickness on membrane degradation and platinum agglomeration under long-term open circuit voltage conditions. Electrochim Acta 2015;153:254–62.

[29] Sugawara S, Maruyama T, Nagahara Y, Kocha SS, Shinohra K, Tsujita K, et al. Performance decay of proton-exchange membrane fuel cells under open circuit conditions induced by membrane decomposition. J Power Sources 2009;187:324–31.

[30] Devrim Y, Arıca ED. Investigation of the effect of graphitized carbon nanotube catalyst support for high temperature PEM fuel cells. Int J Hydrogen Energy 2020;45:3609–17.

[31] Søndergaard T, Cleemann LN, Zhong L, Becker H, Steenberg T, Hjuler HA, et al. Catalyst degradation under potential cycling as an accelerated stress test for PBI-based high-temperature PEM fuel cells—effect of humidification. Electrocatalysis 2018;9:302–13.

[32] Schonvogel D, Rastedt M, Wagner P, Wark M, Dyck A. Impact of accelerated stress tests on high temperature PEMFC degradation. Fuel Cell 2016;16:480–9.

[33] Lin Y. Characterization of phosphoric acid doped polybenzimidazole membranes. Diss. Universitätsbibliothek der RWTH Aachen; 2018.

[34] Wu J, Yuan X, Wang H, Blanco M, Martin J, Zhang J. Diagnostic tools in PEM fuel cell research: Part I

Electrochemical techniques. Int J Hydrogen Energy 2008;33:1735–46.
[35] Zainoodin AM, Tsujiguchi T, Masdar MS, Kamarudin SK, Osaka Y, Kodama A. Performance of a direct formic acid fuel cell fabricated by ultrasonic spraying. Int J Hydrogen Energy 2018;43:6413–20.
[36] Liu S, Rasinski M, Rahim Y, Zhang S, Wippermann K, Reimer U, et al. Influence of operating conditions on the degradation mechanism in high-temperature polymer electrolyte fuel cells. J Power Sources 2019;439.
[37] Hu Z, Xu L, Huang Y, Li J, Ouyang M, Du X, et al. Comprehensive analysis of galvanostatic charge method for fuel cell degradation diagnosis. Appl Energy 2018;212:1321–32.
[38] Zhu H, Li X, Wang F. Synthesis and characterization of Cu@Pt/C core-shell structured catalysts for proton exchange membrane fuel cell. Int J Hydrogen Energy 2011;36:9151–4.
[39] Hwang DS, Park CH, Yi SC, Lee YM. Optimal catalyst layer structure of polymer electrolyte membrane fuel cell. Int J Hydrogen Energy 2011;36:9876–85.
[40] Wippermann K, Elze R, Wannek C, Echsler H, Stolten D. Influence of the ionomer type in direct methanol fuel cell (DMFC) anode catalyst layers on the properties of primary and secondary pores. J Power Sources 2013;228:57–67.
[41] Epting WK, Gelb J, Litster S. Resolving the three-dimensional microstructure of polymer electrolyte fuel cell electrodes using nanometer-scale X-ray computed tomography. Adv Funct Mater 2012;22:555–60.
[42] Park H-S, Cho Y-H, Cho Y-H, Jung CR, Jang JH, Sung Y-E. Performance enhancement of PEMFC through temperature control in catalyst layer fabrication. Electrochim Acta 2007;53:763–7.
[43] Su H, Liang H, Bladergroen BJ, Linkov V, Pollet BG, Pasupathi S. Effect of platinum distribution in dual catalyst layer structured gas diffusion electrode on the performance of high temperature PEMFC. J Electrochem Soc 2014;161:F506–12.
[44] Unnikrishnan A, Rajalakshmi N, Janardhanan VM. Kinetics of electrochemical charge transfer in HT-PEM fuel cells. Electrochim Acta 2019;293:128–40.
[45] Frensch SH, Olesen AC, Araya SS, Kær SK. Model-supported characterization of a PEM water electrolysis cell for the effect of compression. Electrochim Acta 2018;263:228–36.
[46] Reimer U, Lehnert W, Holade Y, Kokoh B. Chapter 2 - irreversible losses in fuel cells. In: Hacker V, Mitsushima S, editors. Fuel cells and hydrogen. Elsevier; 2018. p. 15–40.
[47] Liang H, Su H, Pollet BG, Linkov V, Pasupathi S. Membrane electrode assembly with enhanced platinum utilization for high temperature proton exchange membrane fuel cell prepared by catalyst coating membrane method. J Power Sources 2014;266:107–13.
[48] Winther-Jensen B, MacFarlane DR. New generation, metal-free electrocatalysts for fuel cells, solar cells and water splitting. Energy Environ Sci 2011;4.
[49] Modestov AD, Tarasevich MR, Filimonov VY, Zagudaeva NM. Degradation of high temperature MEA with PBI-H3PO4 membrane in a life test. Electrochim Acta 2009;54:7121–7.
[50] Alvisi M, Galtieri G, Giorgi L, Giorgi R, Serra E, Signore M. Sputter deposition of Pt nanoclusters and thin films on PEM fuel cell electrodes. Surf Coating Technol 2005;200:1325–9.
[51] Yang H, Tang Y, Zou S. Electrochemical removal of surfactants from Pt nanocubes. Electrochem Commun 2014;38:134–7.
[52] He Q, Yang X, Chen W, Mukerjee S, Koel B, Chen S. Influence of phosphate anion adsorption on the kinetics of oxygen electroreduction on low index Pt (hkl) single crystals. Phys Chem Chem Phys 2010;12:12544–55.
[53] Engl T, Gubler L, Schmidt TJ. Catalysts and catalyst-layers in HT-PEMFCs. In: Li Q, Aili D, Hjuler HA, Jensen JO, editors. High temperature polymer electrolyte membrane fuel cells: approaches, status, and perspectives. Cham: Springer International Publishing; 2016. p. 297–313.
[54] Cheng X, Yi B, Han M, Zhang J, Qiao Y, Yu J. Investigation of platinum utilization and morphology in catalyst layer of polymer electrolyte fuel cells. J Power Sources 1999;79:75–81.
[55] Friedmann R, Van Nguyen T. Optimization of the microstructure of the cathode catalyst layer of a PEMFC for two-phase flow. J Electrochem Soc 2010;157:B260–5.
[56] Levie RD. On porous electrodes in electrolyte solutions. Electrochim Acta 1964;9:1231–45.
[57] Maier W, Arlt T, Wippermann K, Wannek C, Manke I, Lehnert W, et al. Correlation of synchrotron X-ray radiography and electrochemical impedance spectroscopy for the investigation of HT-PEFCs. J Electrochem Soc 2012;159:F398–404.
[58] Birry L, Bock C, Xue X, McMillan R, MacDougall B. DMFC electrode preparation, performance and proton conductivity measurements. J Appl Electrochem 2009;39:347–60.
[59] Danzer MA, Hofer EP. Analysis of the electrochemical behaviour of polymer electrolyte fuel cells using simple impedance models. J Power Sources 2009;190:25–33.
[60] Winther-Jensen B, MacFarlane DR. New generation, metal-free electrocatalysts for fuel cells, solar cells and water splitting. Energy Environ Sci 2011;4:2790–8.
[61] Su H, Jao T-C, Barron O, Pollet BG, Pasupathi S. Low platinum loading for high temperature proton exchange membrane fuel cell developed by ultrasonic spray coating technique. J Power Sources 2014;267:155–9.
[62] Lee J, Jung J, Han JY, Kim H-J, Jang JH, Lee H-J, et al. Effect of membrane electrode assembly fabrication method on the single cell performances of polybenzimidazole-based high temperature polymer electrolyte membrane fuel cells. Macromol Res 2014;22:1214–20.
[63] Liu Y, Ji C, Gu W, Baker DR, Jorne J, Gasteiger HA. Proton conduction in PEM fuel cell cathodes: effects of electrode thickness and ionomer equivalent weight. J Electrochem Soc 2010;157:B1154–62.
[64] Liu G, Zhang H, Hu J, Zhai Y, Xu D, Shao Z-g. Studies of performance degradation of a high temperature PEMFC based on H3PO4-doped PBI. J Power Sources 2006;162:547–52.
[65] Reimer U, Schumacher B, Lehnert W. Accelerated degradation of high-temperature polymer electrolyte fuel cells: discussion and empirical modeling. J Electrochem Soc 2015;162:F153–64.
[66] Zhang S, Yuan X-Z, Hin JNC, Wang H, Wu J, Friedrich KA, et al. Effects of open-circuit operation on membrane and catalyst layer degradation in proton exchange membrane fuel cells. J Power Sources 2010;195:1142–8.
[67] Yu S, Xiao L, Benicewicz BC. Durability studies of PBI-based high temperature PEMFCs. Fuel Cell 2008;8:165–74.